JACS
JOURNAL OF THE AMERICAN CHEMICAL SOCIETY

ARTICLE

pubs.acs.org/JACS

Spin Diffusion Driven by R-Symmetry Sequences: Applications to Homonuclear Correlation Spectroscopy in MAS NMR of Biological and Organic Solids

Guangjin Hou,[†,‡] Si Yan,[†] Shangjin Sun,[†] Yun Han,[†,‡] In-Ja L. Byeon,[‡,§] Jinwoo Ahn,[‡,§] Jason Concel,[‡,§] Ago Samoson,[∥,⊥] Angela M. Gronenborn,[‡,§] and Tatyana Polenova[†,‡,*]

[†]Department of Chemistry and Biochemistry, University of Delaware, Newark, Delaware 19716, United States

[‡]Pittsburgh Center for HIV Protein Interactions, University of Pittsburgh School of Medicine, 1051 Biomedical Science Tower 3, 3501 Fifth Avenue, Pittsburgh, Pennsylvania 15261, United States

[§]Department of Structural Biology, University of Pittsburgh School of Medicine, 1051 Biomedical Science Tower 3, 3501 Fifth Avenue, Pittsburgh, Pennsylvania 15261, United States

[∥]Tallinn University of Technology, Ehitajate tee 5, 19086, Tallinn, Estonia

[⊥]Physics Department, University of Warwick, Coventry, United Kingdom

Supporting Information

ABSTRACT: We present a family of homonuclear $^{13}C-^{13}C$ magic angle spinning spin diffusion experiments, based on $R2_n^{\nu}$ (n = 1 and 2, ν = 1 and 2) symmetry sequences. These experiments are well suited for $^{13}C-^{13}C$ correlation spectroscopy in biological and organic systems and are especially advantageous at very fast MAS conditions, where conventional PDSD and DARR experiments fail. At very fast MAS frequencies the $R2_1^1$, $R2_2^1$, and $R2_2^2$ sequences result in excellent quality correlation spectra both in model compounds and in proteins. Under these conditions, individual $R2_n^{\nu}$ display different polarization transfer efficiency dependencies on isotropic chemical shift differences: $R2_2^1$ recouples efficiently both small and large chemical shift differences (in proteins these correspond to aliphatic-to-aliphatic and carbonyl-to-aliphatic correlations, respectively), while $R2_1^1$ and $R2_2^2$ exhibit the maximum recoupling efficiency for the aliphatic-to-aliphatic or carbonyl-to-aliphatic correlations, respectively. At moderate MAS frequencies (10−20 kHz), all $R2_n^{\nu}$ sequences introduced in this work display similar transfer efficiencies, and their performance is very similar to that of PDSD and DARR. Polarization transfer dynamics and chemical shift dependencies of these R2-driven spin diffusion (RDSD) schemes are experimentally evaluated and investigated by numerical simulations for [U−^{13}C,^{15}N]-alanine and the [U−^{13}C,^{15}N] *N*-formyl-Met-Leu-Phe (MLF) tripeptide. Further applications of this approach are illustrated for several proteins: spherical assemblies of HIV-1 U−^{13}C,^{15}N CA protein, U−^{13}C,^{15}N-enriched dynein light chain DLC8, and sparsely ^{13}C/uniformly ^{15}N enriched CAP-Gly domain of dynactin. Due to the excellent performance and ease of implementation, the presented $R2_n^{\nu}$ symmetry sequences are expected to be of wide applicability in studies of proteins and protein assemblies as well as other organic solids by MAS NMR spectroscopy.

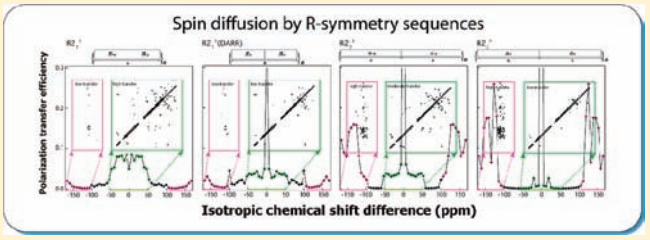

INTRODUCTION

With the recent developments in decoupling and recoupling techniques, solid-state NMR has become a powerful tool for determining molecular structure and dynamics in biological solids, ranging from amyloid fibrils to membrane proteins to intact viruses to protein assemblies.[1−10] Magic angle spinning (MAS) recoupling methods, both dipolar and scalar based, have emerged as an essential tool for structural and dynamics characterization of uniformly and extensively enriched biopolymers.[11−24] With the recent breakthroughs in probe technology, very fast MAS frequencies of the order of 40−70 kHz are now accessible to the experimentalist,[25−27] and these fast MAS conditions result in greatly enhanced spectral resolution due to efficient averaging of the homonuclear $^1H-^1H$ dipolar interactions at spinning rates above 30 kHz and due to efficient heteronuclear ^1H-X decoupling that can be achieved at high rotation frequencies. The narrow ^1H lines under very fast MAS also permit proton detection, and indeed, several investigators have recently demonstrated the benefits of proton-detected experiments in proteins, both in terms of greatly enhanced sensitivity and the additional information that can be gained by incorporating the proton dimension into the spectra.[28−31] In the heteronucleus-detected experiments, the narrow lines attained

Received: September 24, 2010
Published: March 01, 2011

at very fast MAS frequencies also give rise to significant sensitivity enhancements, and therefore, very fast MAS conditions are in principle advantageous across the board for structural and dynamics studies of proteins and protein assemblies. However, implementation of fast-MAS protocols for protein structure determination requires the development of modified homo- and heteronuclear recoupling methods[26,32−36] because many of the recoupling techniques that are commonly employed at MAS frequencies below 20 kHz do not work above 30 kHz.

Types of experiments that do not work in their original implementation under very fast MAS conditions comprise homonuclear spin-diffusion-based recoupling methods, such as proton-driven spin diffusion (PDSD)[37,38] and dipolar-assisted rotational resonance (DARR)[20,39] or RF-assisted diffusion (RAD).[40] These techniques are ubiquitously used in structural analysis of proteins and protein assemblies at moderate MAS frequencies (10−20 kHz), both for resonance assignments and for deriving long-range distance constraints as well as for quantitative CP/MAS measurements.[1,6,7,11,12,22,23,41−57] These sequences are some of the very few homonuclear recoupling methods (along with PAR[34,58,59] and CHHC[60,61]) that do not suffer from dipolar truncation[36,44,62−64] and are thus particularly advantageous for extracting distance information in uniformly and extensively enriched proteins.

In PDSD experiments, the recoupling efficiency depends strongly on the line broadening due to the residual ^{1}H−X dipolar couplings and on the spinning frequency, and in some cases it is hard to achieve broad-band homonuclear correlation spectra. This limitation is alleviated when a weak radio frequency (rf) field irradiation is applied on the protons during the mixing time, such as in DARR (RAD) experiments. For DARR (RAD) irradiation, the ^{1}H rf field strength is $\omega_{1H} = n\omega_r$, satisfying the rotary resonance matching condition and resulting in broad-band rotational resonance recoupling. During the mixing time, ^{13}C−^{13}C polarization transfer is driven by the reintroduced ^{1}H−^{13}C and ^{1}H−^{1}H dipolar couplings, and the transfer efficiency for the coupled ^{13}C spins is somewhat less dependent on MAS frequency than in the conventional PDSD experiment. While dependence of polarization transfer efficiency on the MAS frequency in DARR (RAD) experiments is not as dramatic as in the PDSD sequence, the dependence on the chemical shift difference between the coupled spins is very strong.[65] This chemical shift difference dependence is particularly severe at very fast MAS rates (>30 kHz), resulting in lower and nonuniform polarization transfer efficiencies across the spectrum, and at frequencies of 40 kHz or above DARR/RAD would not be a method of choice for ^{13}C correlation spectroscopy.

Recently, several amplitude- and phase-modulated DARR/RAD experiments were developed to improve the spin diffusion efficiency under very fast MAS conditions.[36,65,66] Second-order rotational resonance conditions, $\omega_1 = n\omega_r \pm \Delta\omega_{iso}$, were introduced by Ernst et al.[36] Broad-band homonuclear dipolar recoupling at very fast MAS frequencies can be performed by various amplitude-modulated ^{1}H rf field irradiation schemes, referred to as mixed rotational and rotary-resonance (MIRROR) technique. Tekely et al. proposed a phase-alternated recoupling irradiation (PARIS)[66,67] scheme to obtain more efficient polarization transfer at very fast MAS, and the phase-alternated DARR irradiation compensates efficiently for rf field inhomogeneity and improves the magnetization transfer rate. Nevertheless, the chemical shift offset sensitivity still remains an issue in these sequences, and it is difficult to achieve uniform broad-band polarization transfer.

In this work, we present a family of spin diffusion experiments in which the magnetization transfer is driven by rotor-synchronized R2$_n^\nu$ symmetry-based recoupling. Such symmetry-based approaches in MAS recoupling pulse sequences were originally described by Levitt in a series of elegant studies that established the general design principles for these sequences as well as classified them as CN_n^ν and RN_n^ν schemes depending on the rotation properties of the spin angular momenta during the rotor-synchronized train of rf pulses.[68−71] RN_n^ν-type sequences, employed in this work, are designed to produce a net rotation of the spin angular momenta by π around the x axis of the rotating frame.[68] Following the Levitt nomenclature, n and ν are small integers and referred to as the symmetry numbers of the pulse sequence. In the R2$_n^\nu$ symmetry-based spin diffusion experiments introduced here, all pairwise combinations of n = 1, 2 and ν = 1, 2 are employed to produce four sequences, R2$_1^1$, R2$_1^2$, R2$_2^1$, and R2$_2^2$. The pulse element of the R2 symmetry sequences can be either a basic π pulse or composite pulses such as $90°_x90°_y90°_x$, $90°_x270°_{-x}$, or $90°_x180°_y90°_x$. In these R2 sequences, the rf field amplitude and phase alternation are defined according to the R-type symmetry. It should be noted that the basic R2$_1^1$ symmetry scheme has the same pulse type as the rotor-synchronized PARIS[66] scheme and that the basic R2$_1^2$ symmetry scheme has the same pulse type as the conventional DARR/RAD scheme. We demonstrate that these different R2-driven spin diffusion schemes (RDSD) exhibit similar transfer efficiencies at moderate MAS rates (<20 kHz) except that R2$_1^1$ and POST-R2$_2^1$ are advantageous for the recoupling of coupled spins with large chemical shift differences. At very fast MAS frequencies, the individual R2 irradiation schemes display distinct dependencies of the polarization transfer efficiencies on the chemical shift differences between coupled carbon spins. Experiments and numerical simulations in [U−^{13}C,^{15}N]-alanine and [U−^{13}C,^{15}N] *N*-formyl-Met-Leu-Phe (MLF) tripeptide indicate that under very fast MAS the polarization transfer in these R2$_n^\nu$ spin diffusion experiments is driven by the broadened second-order rotational resonance condition ($\omega_1 \pm n\omega_r - K_{sc}\omega_{DD} \leq \Delta\omega_{iso} \leq \omega_1 \pm n\omega_r + K_{sc}\omega_{DD}$), and we present the theoretical treatment of these sequences that correctly accounts for the polarization transfer dynamics and for the observed chemical shift dependence of the individual R2$_n^\nu$ schemes. Our results further indicate that due to these distinct chemical shift dependencies it is advantageous to employ a specific R2 sequence for a given correlation experiment, e.g., CACB vs CACO.

We further demonstrate that these R2$_n^\nu$ spin diffusion sequences perform very efficiently in proteins and protein assemblies using three examples: spherical assemblies of U−^{13}C,^{15}N-enriched HIV-1 CA protein, U−^{13}C,^{15}N-enriched dynein light chain DLC8, and sparsely-^{13}C/U−^{15}N-labeled dynactin CAP-Gly domain. We anticipate that the approach presented here for R2$_n^\nu$ spin diffusion under fast-MAS conditions will be broadly applicable to studies of proteins and protein assemblies by MAS NMR spectroscopy, which is a rapidly growing area of research.

EXPERIMENTS AND METHODS

Samples. [U−^{13}C,^{15}N]-alanine and [U−^{13}C,^{15}N] *N*-formyl-Met-Leu-Phe (MLF) tripeptide were purchased from Cambridge Isotope Laboratories. Both powder samples were used in the subsequent NMR experiments without any further purification or recrystallization.

The sample of spherical assemblies of U−^{13}C,^{15}N-enriched HIV-1 capsid protein (CA) was prepared according to established procedures.[6] CAP-Gly sparsely enriched in ^{13}C and uniformly labeled with ^{15}N was prepared from *E. coli*, grown in minimal medium containing 1,3-^{13}C glycerol (Cambridge Isotopes) as the sole carbon source and $^{15}NH_4Cl$ as the sole nitrogen source, as described previously.[72−74] The solid-state NMR sample of CAP-Gly was prepared by controlled precipitation from polyethylene glycol,[36,44,62,63] slowly adding a solution of 30% PEG-3350 to the solution of 24.3 mg of CAP-Gly (38.5 mg/mL), both dissolved in 10 mM MES buffer (10 mM $MgCl_2$, pH 6.0), as described previously.[7] U−^{13}C, ^{15}N-enriched dynein light chain protein (DLC8) was expressed in *E. coli* and purified as described previously.[75] The solid-state NMR sample of DLC8 was prepared by controlled precipitation, slowly adding a solution of 30% PEG-3350 to the solution of 11 mg of DLC8 (30 mg/mL). Prior to the precipitation step, both PEG-3350 and DLC8 were dissolved in 10 mM MES buffer (10 mM $MgCl_2$, pH 6.0) and doped with 50 mM EDTA−Cu(II). The protein samples were packed in 1.8 mm MAS rotors for solid-state NMR experiments.

Solid-State NMR Spectroscopy. All NMR experiments were carried out on a Varian InfinityPlus solid-state NMR spectrometer operating at a Larmor frequency of 599.8 MHz for ^{1}H and 150.8 MHz for ^{13}C. Solid-state NMR experiments were performed using either a 3.2 mm Varian triple-resonance T3 probe (spinning rates of up to 25 kHz) or a 1.8 mm MAS triple-resonance probe developed in the Samoson laboratory (spinning rates up to 50 kHz).

The pulse schemes for RDSD 2D experiments are shown in Figure 1. During the mixing period, a series of $R2_n^{\nu}$ symmetry pulses is applied on the ^{1}H channel, as illustrated in Figure 1b−e for each specific $R2_n^{\nu}$ experiment. For $R2_1^{\nu}$ symmetry irradiation, the rf field strength equals the MAS frequency and one rotor period contains two π pulses. For $R2_2^{\nu}$ symmetry irradiation, the rf field strength equals one-half the MAS frequency and one rotor period contains one π pulse. For POST-$R2_n^{\nu}$ symmetry irradiation, the basic π pulse is replaced by a composite pulse, $(\pi/2)_0(3\pi/2)_{180}$, and the rf field strength is twice that of the $R2_n^{\nu}$ symmetry irradiation, as shown in Figure 1f for POST $R2_2^1$.

NMR experiments on the MLF sample packed into a 3.2 mm rotor were recorded at room temperature and a MAS frequency of 16 kHz. Typical 90° pulse lengths were 2.8 μs for ^{1}H and 4.0 μs for ^{13}C. The cross-polarization contact time was 1.4 ms, and the recycle delay was 3.0 s. Two-pulse phase-modulation (TPPM)[76] ^{1}H decoupling with an rf field strength of 96 kHz was performed during the acquisition, and continuous wave (CW) ^{1}H decoupling with the same rf field strength was applied during the t_1 evolution time. ^{1}H irradiation with an rf field strength of 16 and 8 kHz during the mixing time was applied for 2D $R2_1^{\nu}$ and $R2_2^{\nu}$ ($\nu = 1, 2$) correlation experiments, respectively. The 2D spectra were collected as (1000 × 256) (complex × real) matrices with 8 scans; the TPPI (time proportional phase incrementation) scheme was used for phase-sensitive detection in the indirect dimension.[77] A series of experiments with different mixing times ranging between 1 and 50 ms was performed.

NMR experiments on an alanine sample packed into a 1.8 mm rotor were performed at the MAS frequency of 40 kHz. To reduce sample heating during fast MAS spinning, nitrogen gas at 0 °C was used for cooling, resulting in a final sample temperature of 20 °C. The rf field strength on the ^{1}H channel during the mixing time was 40 and 20 kHz for $R2_1^{\nu}$ and $R2_2^{\nu}$ experiments, respectively. CW ^{1}H decoupling with a rf field strength of 9 kHz was employed in the t_1 and t_2 dimensions. The 2D spectra were collected as (2000 × 512) (complex × real) matrices with 8 scans; the TPPI scheme was used for phase-sensitive detection in the indirect dimension. A series of experiments with different mixing times ranging between 5 and 500 ms were performed.

NMR experiments on protein samples packed into a 1.8 mm rotor were performed at the MAS frequencies of 10 and 40 kHz. To reduce the sample heating due to fast MAS spinning at 40 kHz, a stream of cooling nitrogen gas at −20, −25, and −35 °C was used for the HIV-1 CA, CAP-Gly, and DLC8 samples, resulting in final sample temperatures of 0, −5, and −15 °C, respectively. For all 2D $R2_n^{\nu}$ ^{13}C−^{13}C correlation experiments, the TPPI scheme was used for phase-sensitive detection in the indirect t_1 dimension. The other parameters were the same as those used for the experiments on alanine. For all RDSD NMR experiments conducted at the MAS frequency of 10 kHz, a 96 kHz ^{1}H TPPM decoupling was applied during t_1 and t_2. Detailed acquisition and procession parameters are shown in the Supporting Information.

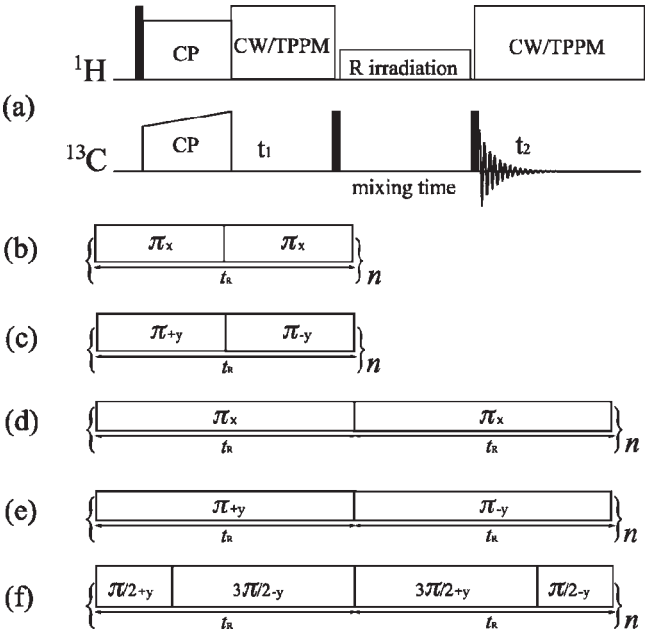

Figure 1. (a) The general pulse sequence for 2D ^{13}C−^{13}C $R2_n^{\nu}$ homonuclear correlation experiments. An RF field irradiation is applied on proton spins during the mixing time. RG irradiation represents rotor-synchronized R2-type symmetry pulses: (b) $R2_1^2$ ($\omega_{rf} = \omega_r$), (c) $R2_1^1$ ($\omega_{rf} = \omega_r$), (d) $R2_2^2$ ($\omega_{rf} = 1/2\ \omega_r$), (e) $R2_2^1$ ($\omega_{rf} = 1/2\ \omega_r$), and (f) POST $R2_2^1$ ($\omega_{rf} = \omega_r$).

Numerical Simulations. All numerical simulations were performed in SIMPSON.[78] One hundred sixty eight REPULSION (α, β) angles and 16 γ angles were used to generate a powder average. The atomic coordinates for the model spin systems employed in the simulations were taken from the SSNMR structure of the leucine residue in the *N*-f-MLF-OH tripeptide (PDB ID 1Q7O).[50] These atomic coordinates are generally regarded as a valid representation for spin systems of other amino acids. For C_α−C′ spin diffusion simulations, a spin cluster containing two carbons and one proton was used. For C_α−C_β spin diffusion simulations, a spin cluster containing two carbons and three protons was employed. The one-bond dipolar coupling constants for ^{1}H−^{13}C and ^{13}C−^{13}C were 22 690 and 2251 Hz, respectively. In all simulations, all possible pairwise dipolar couplings were taken into account. *J* couplings were ignored as their effects are negligible given their small size. Other parameters used in simulations were the same as in the corresponding experiments.

RESULTS AND DISCUSSION

Symmetry-Based Spin Diffusion Experiments at Moderate MAS Frequencies. $R2_n^{\nu}$ symmetry-based pulse irradiation on protons can be used to reintroduce hetero- and homonuclear dipolar couplings, which in turn allow for spin diffusion among carbon spins. The space-spin selection rules for the symmetry-allowed first-order average Hamiltonian terms have been

dx.doi.org/10.1021/ja108650x |*J. Am. Chem. Soc.* 2011, 133, 3943–3953

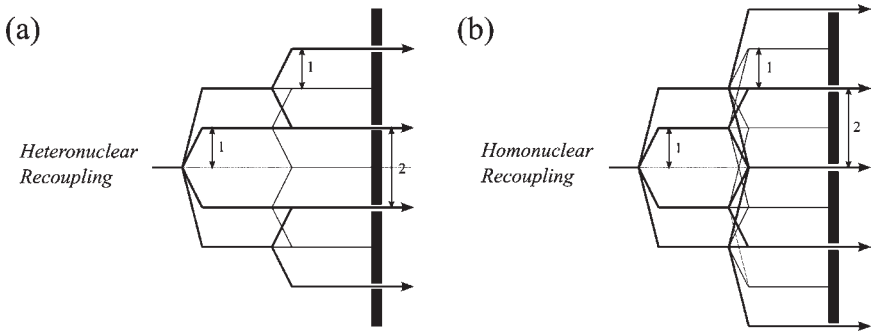

Figure 2. Space−spin selection diagrams for the first-order average dipolar Hamiltonian in the $R2_1^1$ symmetry sequence for recoupling of I−S heteronuclear terms (a) and I−I homonuclear terms (b).

Table 1. Total Number of Symmetry-Allowed First- and Second-Order Average Hamiltonian Terms in the $R2_n^\nu$ (n, ν = 1 and 2) Symmetry Sequences

	no. of symmetry-allowed terms			
symmetry sequences	$\bar{H}_{IS}^{(1)}$	$\bar{H}_{II}^{(1)}$	$\bar{H}_{I\times IS}^{(2)}$	$\bar{H}_{II\times IS}^{(2)}$
$R2_1^2$	6	10	96	208
$R2_1^1$	6	10	96	208
$R2_2^2$	0	20	96	208
$R2_2^1$	8	12	96	208

reported elsewhere.[68] Figure 2 demonstrates space−spin selection diagrams for the interaction Hamiltonians in the $R2_1^1$ sequence. It can be seen that both the $^1H-^{13}C$ heteronuclear dipolar couplings and the $^1H-^1H$ homonuclear dipolar couplings are reintroduced by the $R2_1^1$ symmetry irradiation, with 6 heteronuclear dipolar coupling terms $H_{IS}^{(1)}$ and 10 homonuclear dipolar coupling terms $H_{II}^{(1)}$ of the first-order average Hamiltonian being symmetry allowed. Even though spin diffusion between coupled ^{13}C spins is primarily determined by the $^{13}C-^{13}C$ coupling strength and the first-order rotational resonance conditions ($n\omega_r = \Delta\omega_{iso}$), the reintroduced $^1H-^{13}C$ and $^1H-^1H$ dipolar couplings represent an essential contribution, resulting in greatly broadened RR matching conditions. Furthermore, these dipolar couplings also contain the second-order average Hamiltonian terms. Even though the recoupled second-order average Hamiltonian terms are much smaller than the first-order contributions, they can also drive the $^1H-^{13}C$ and $^1H-^1H$ cross relaxation and assist the $^{13}C-^{13}C$ spin diffusion. Table 1 summarizes the number of the first- and second-order average Hamiltonian terms in the $R2_n^\nu$ symmetry sequences. These recoupled hetero- and homonuclear dipolar Hamiltonian terms would drive the polarization transfer (see the Supporting Information for details on the recoupled terms for each $R2_n^\nu$ sequence). The first-order rotational resonance conditions would be broadened greatly by $R2_n^\nu$ reintroduced dipolar interactions, and these can be expressed as $n\omega_r - K_{sc}\omega_{DD} \le \Delta\omega_{iso} \le \pm n\omega_r + K_{sc}\omega_{DD}$, where $K_{sc}\omega_{DD}$ denotes the size of the recoupled dipolar interactions by $R2_n^\nu$ and K_{sc} is the corresponding scaling factor.

It is obvious from Table 1 that the number of the symmetry-allowed Hamiltonian terms is different for each recoupling sequence, except for $R2_1^2$ and $R2_1^1$. Even though for $R2_1^2$ and $R2_1^1$ the same number of first- and second-order Hamiltonian terms are symmetry allowed, the nature of these recoupled

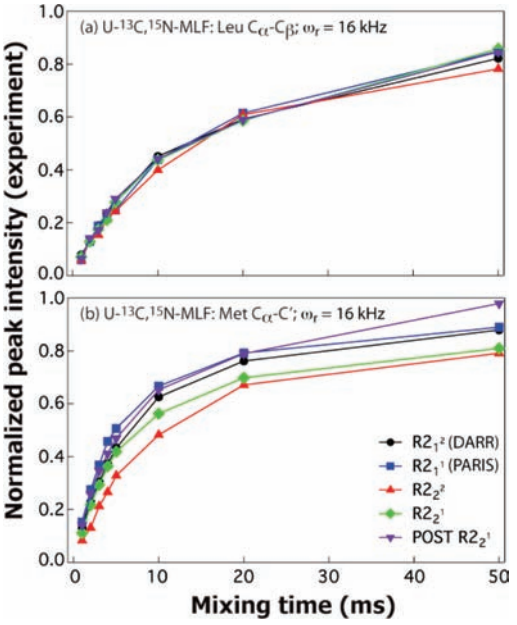

Figure 3. Polarization transfer in the 2D $R2_n^\nu$-driven (n, ν = 1 and 2) spin diffusion experiments as a function of the mixing time for (a) $C_\alpha-C_\beta$ of Leu residue and (b) $C_\alpha-C'$ of Met residue in [U−^{13}C,^{15}N] *N*-formyl-Met-Leu-Phe (MLF) tripeptide. The sample was spun at a MAS frequency of 16 kHz. The cross-peak intensities in each spectrum were normalized to those of the corresponding diagonal peaks in the following way: $I_{norm}=(2I_{AB})/(I_{AA}+I_{BB})$, where I_{norm} is the normalized cross peak intensity, I_{AB} is the non-normalized cross peak intensity, and I_{AA} and I_{BB} are the non-normalized intensities of the corresponding diagonal peaks. The build-up curves corresponding to the different recoupling sequences are color coded as follows: $R2_1^2$, black; $R2_1^1$, blue; $R2_2^2$, red; $R2_2^1$, green; and POST-$R2_2^1$, purple.

Hamiltonian terms {l, *m*, *λ*, *μ*} as well as the corresponding scaling factors are totally different (see the Supporting Information), suggesting that different polarization transfer dynamics might be observed in the corresponding spin diffusion experiments. To examine the $^{13}C-^{13}C$ transfer rates in each specific sequence at moderate MAS frequencies, we recorded a series of two-dimensional $R2_n^\nu$ (n, ν = 1 and 2) correlation spectra with varying mixing times in the MLF tripeptide. The $^{13}C-^{13}C$ polarization transfer build-up curves acquired at the MAS frequency of 16 kHz are illustrated in Figure 3a for the $C_\alpha-C_\beta$ correlation of Leu residue and in Figure 3b for the $C_\alpha-C'$ correlation of Met residue.

dx.doi.org/10.1021/ja108650x |*J. Am. Chem. Soc.* 2011, 133, 3943–3953

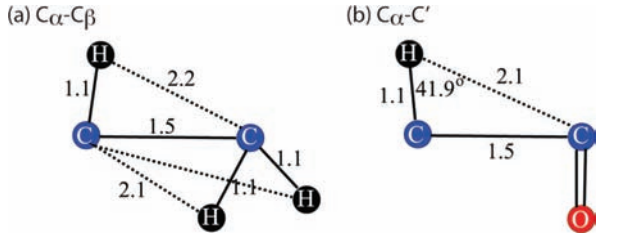

Figure 4. Spin models for numerical simulations of the polarization transfer dynamics in the $R2_n^{\nu}$ symmetry-driven sequences: (a) $C_\alpha-C_\beta$ spin system (three protons and two carbons) and (b) $C_\alpha-C'$ spin system (one proton and two carbons). The atomic coordinates were obtained from the SSNMR structure of MLF.[50] The interatomic distances are indicated in the figure. The oxygen atom was not taken into account in the simulations.

The results demonstrate that despite the different number of symmetry-allowed Hamiltonian terms in each of the $R2_n^{\nu}$ symmetry-based schemes, all of these sequences exhibit similar polarization transfer efficiencies and polarization transfer rates for $C_\alpha-C_\beta$ correlations at moderate spinning frequencies. On the other hand, for the $C_\alpha-C'$ correlation, the $R2_1^1$ scheme shows a slightly higher polarization transfer rate than the other sequences. We also note that as expected, the POST versions of sequences in which the basic π pulse of the R element is replaced with composite (90_0270_{180}) pulses, display improved transfer efficiency in the $^{13}C-^{13}C$ correlation experiments, especially for coupled ^{13}C spins with large chemical shift differences.

Symmetry-Based Spin Diffusion Experiments at Very Fast MAS Frequencies: Alanine. Either proton-driven or dipolar-assisted spin diffusion can be used to perform broad-band homonuclear correlation experiments, but both of these recoupling methods display low tolerance to large resonance frequency offsets, which are most pronounced at fast and very fast MAS rates (>30 kHz). Since we found that at moderate MAS frequencies the performance of the $R2_n^{\nu}$ symmetry-driven sequences is largely independent of the chemical shift offset between the coupled spins, we proceeded with examining the spin diffusion behavior of these sequences at very fast MAS frequencies. Two idealized models of dipolar-coupled spin networks were constructed that represent the smallest coupled C−C spin systems in proteins using the atomic coordinates of the leucine residue in *N*-f-MLF-OH, as shown in Figure 4. We used these models in the numerical simulations to evaluate the $^{13}C_\alpha-^{13}C_\beta$ and $^{13}C_\alpha-^{13}C'$ polarization transfer dynamics.

Figure 5 demonstrates the $^{13}C-^{13}C$ polarization transfer dynamics by basic (solid curves) and POST (dotted or dashed curves) $R2_n^{\nu}$ symmetry sequences simulated for the above model spin systems at the MAS frequency of 40 kHz. The build-up curves for the $C_\alpha-C_\beta$ and $C_\alpha-C'$ correlations are shown in Figure 5a and 5b, respectively. As can be appreciated, under the very fast MAS conditions, the various $R2_n^{\nu}$ symmetry-driven schemes exhibit very different polarization transfer dynamics, depending greatly on the chemical shift difference between the coupled ^{13}C spins. For the $C_\alpha-C'$ polarization transfer by the basic $R2_n^{\nu}$, the $R2_2^2$ sequence with an rf field irradiation of 20 kHz exhibits the fastest polarization transfer rate. On the other hand, there is almost no $C_\alpha-C'$ polarization transfer observed for the $R2_1^{\nu}$ (ν = 1, 2) sequences with rf field irradiation of 40 kHz. At the same time, for the $C_\alpha-C_\beta$ recoupling, the $R2_1^1$ symmetry scheme yields the most efficient polarization transfer. Even though the $C_\alpha-C_\beta$ polarization transfer can also be

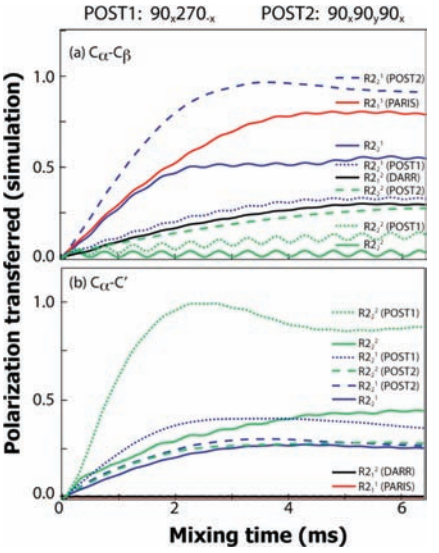

Figure 5. Simulated polarization build-up curves for different $R2_n^{\nu}$ and POST $R2_2^{\nu}$ recoupling sequences for (a) $C_\alpha-C_\beta$ and (b) $C_\alpha-C'$ correlations. Spin models shown in Figure 4a and 4b were used for $C_\alpha-C_\beta$ and $C_\alpha-C'$ simulations, respectively. The ^1H Larmor frequency was 599.8 MHz. The MAS frequency was 40 kHz. The solid build-up curves corresponding to the different basic $R2_n^{\nu}$ recoupling sequences are color coded as follows: $R2_1^1$, red; $R2_1^2$, black; $R2_2^1$, blue; and $R2_2^2$, green. The dotted and dashed curves correspond to POST-type symmetry sequences with composite pulses $90°_x270°_{-x}$ (POST1), and $90°_x90°_y90°_x$ (POST2), respectively.

accomplished with the $R2_2^2$ sequence, the transfer rate is significantly slower. Confirming the experimental results, the current numerical simulations indicate that DARR (referred to as $R2_1^2$ symmetry sequence here) is inefficient for polarization transfer at high MAS frequencies; furthermore, it is very sensitive to the chemical shift differences, rendering DARR experiments impractical under these conditions.

As discussed above, replacement of the basic π pulse by composite pulses gives rise to the various POST $R2_n^{\nu}$ symmetry sequences, and some of these are expected to yield higher transfer efficiency with the appropriate selection of composite pulses. For example, for $C_\alpha-C_\beta$ polarization transfer, POST $R2_2^1$ symmetry sequence consisting of $(90_x90_y90_x)$ composite pulses, exhibits transfer efficiency much higher than the basic $R2_1^1$ scheme. In the case of $C_\alpha-C'$ recoupling, the POST $R2_2^2$ symmetry sequence, consisting of (90_x270_{-x}) composite pulses, exhibits a much higher transfer efficiency than the basic $R2_2^2$ scheme. It should be noted, however, that not all POST $R2_n^{\nu}$ sequences perform better than the basic $R2_n^{\nu}$ schemes. For instance, the POST $R2_2^1$ symmetry sequence, consisting of (90_x270_{-x}) composite pulses, has a lower transfer efficiency than the basic $R2_2^1$ scheme for the $C_\alpha-C_\beta$ polarization transfer.

In order to understand the behavior of the $R2_n^{\nu}$ symmetry-driven sequences as a function of the MAS frequency and the chemical shift difference, one needs to further consider the various factors important in the polarization transfer dynamics. For example, at low or moderate MAS frequencies, DARR (or $R2_1^2$ symmetry sequence) can be regarded as a broad-band rotary resonance (RR) based recoupling technique, since the first-order RR matching conditions are broadened greatly by the reintroduced $^1H-^{13}C$ dipolar couplings. Following this logic, one might think that at very fast MAS frequencies, the transfer

dx.doi.org/10.1021/ja108650x |*J. Am. Chem. Soc.* 2011, 133, 3943–3953

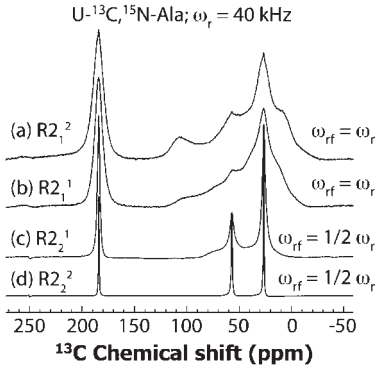

Figure 6. 1D ^{13}C CP/MAS spectra of [U−^{13}C,^{15}N]-alanine spun at 40 kHz. These spectra were recorded with (a) $R2_1^2$, (b) $R2_1^1$, (c) $R2_2^1$, and (d) $R2_2^2$ irradiation applied to the protons during the acquisition period.

efficiency in the DARR experiments may be poor since the partly recoupled heteronuclear dipolar interactions are not strong enough to satisfy the first-order RR matching condition. To investigate this possibility, we examined the extent of dipolar broadening by DARR and by other $R2_n^\nu$ symmetry sequences at the MAS frequency of 40 kHz. Figure 6 shows the experimental ^{13}C CP/MAS spectra of alanine spun at 40 kHz, recorded with the ^1H rf field irradiation during the acquisition period by (Figure 6a) $R2_1^2$ (DARR), (Figure 6b) $R2_1^1$, (Figure 6c) $R2_2^1$, and (Figure 6d) $R2_2^2$ symmetry pulses. The results show that ^{13}C NMR lines are strongly broadened in the 1D $R2_1^\nu$ experiments (Figure 6 a and 6b) and that the line shapes for these two cases are similar because both sequences have the same number of symmetry-allowed Hamiltonian terms (see Table 1). Interestingly, even though the $R2_2^1$ symmetry scheme retains the largest number of symmetry-allowed $^1H-^{13}C$ and $^1H-^1H$ Hamiltonian terms, the broadening of the ^{13}C NMR resonances by the $R2_2^1$ irradiation is much smaller than that by the $R2_1^1$ and $R2_1^2$ sequences. This is the result of the smaller scaling factor for recoupling of the heteronuclear dipolar couplings by $R2_2^1$. Since no first-order average $^1H-^{13}C$ dipolar Hamiltonian terms are allowed in the $R2_2^2$ symmetry scheme (see Table 1), the ^{13}C MAS spectrum exhibiting the least broadening in the presence of the ^1H rf field is obtained.

It is clear from the above discussion that ^{13}C MAS spectra acquired with the various $R2_n^\nu$ irradiation sequences are broadened to different degrees, and in the case of $R2_2^2$ irradiation, no broadening from the recoupled first-order average Hamiltonian interactions ensues. However, these reintroduced dipolar couplings cannot broaden efficiently the first-order rotational resonance conditions ($n\omega_r = \Delta\omega_{iso}$) under very fast MAS, and the polarization transfer profile depends to a greater extent on the second-order rotational resonance conditions ($\omega_1 = n\omega_r \pm \Delta\omega_{iso}$).[36] The strength of the rf field irradiation and the size of the recoupled dipolar couplings would jointly dominate the polarization transfer. The degree of broadening in the different $R2_n^\nu$ symmetry sequences, therefore, does not directly correspond to the polarization transfer efficiencies, indicating that the dipolar broadening is not the dominant factor in spin diffusion experiments.

Figure 7 provides the experimental $^{13}C-^{13}C$ polarization transfer dynamics in the various $R2_n^\nu$ symmetry-driven spin diffusion experiments for U−^{13}C, ^{15}N-alanine, spun at 40 kHz. The $C_\alpha-C_\beta$ and $C_\alpha-C'$ build-up curves are plotted in Figure 7 a and 7b, respectively. The results demonstrate that the $R2_1^1$

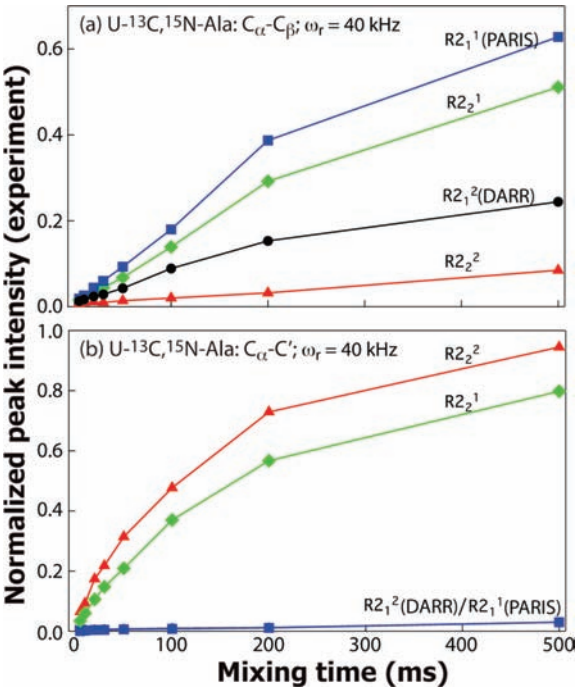

Figure 7. Experimental build-up curves for polarization transfer in U−^{13}C, ^{15}N alanine: (a) $C_\alpha-C_\beta$ and (b) $C_\alpha-C'$ by $R2_1^2$, $R2_1^1$, $R2_2^1$, and $R2_2^2$ symmetry-based sequences. The sample was spun at a MAS frequency of 40 kHz. The cross-peak intensities in each spectrum were normalized to those of the corresponding diagonal peaks in the following way: $I_{norm} = (2I_{AB})/(I_{AA} + I_{BB})$, where I_{norm} is the normalized cross peak intensity, I_{AB} is the non-normalized cross peak intensity, and I_{AA} and I_{BB} are the non-normalized intensities of the corresponding diagonal peaks.

sequence exhibits the most efficient polarization transfer for the $C_\alpha-C_\beta$ spin diffusion experiments. For the $C_\alpha-C'$ polarization transfer, the $R2_2^\nu$ sequences yields much higher transfer rates than the $R2_1^\nu$ symmetry sequences. This finding is consistent with the simulation results shown in Figure 5 except for the differences in the transfer rates, which can be attributed to relaxation effects. Various cross-relaxation times, such as T_1^{HH}, T_1^{HC}, and T_1^{CC} contribute to the magnetization transfer process and were not taken into account in SIMPSON simulations. However, disregarding these relaxation times in the numerical simulations does not affect the comparison of the performances of the different R symmetry sequences, as demonstrated experimentally on protein samples (see below). Despite the difference in the absolute transfer rates between the experimental and the simulated data the relative polarization transfer dynamics between the different R2 sequences is captured correctly in the simulations.

It should be noted that although the $R2_1^2$ scheme (DARR or RAD) resulted in the largest broadening of the ^{13}C lines (Figure 6 and discussed above), the DARR polarization transfer efficiency at very fast MAS frequencies is very low, especially for the $C^\alpha-C'$ correlation experiments, since neither the first-order ($n\omega_r = \Delta\omega_{iso}$) nor the second-order ($\omega_1 = n\omega_r \pm \Delta\omega_{iso}$) rotary resonance conditions are fulfilled at the MAS frequency of 40 kHz. In other words, the $^1H-^{13}C$ heteronuclear dipolar couplings are no longer the primary factor in creating uniform $^{13}C-^{13}C$ polarization transfer at very fast MAS frequencies, and the polarization transfer profile depends on the rf field

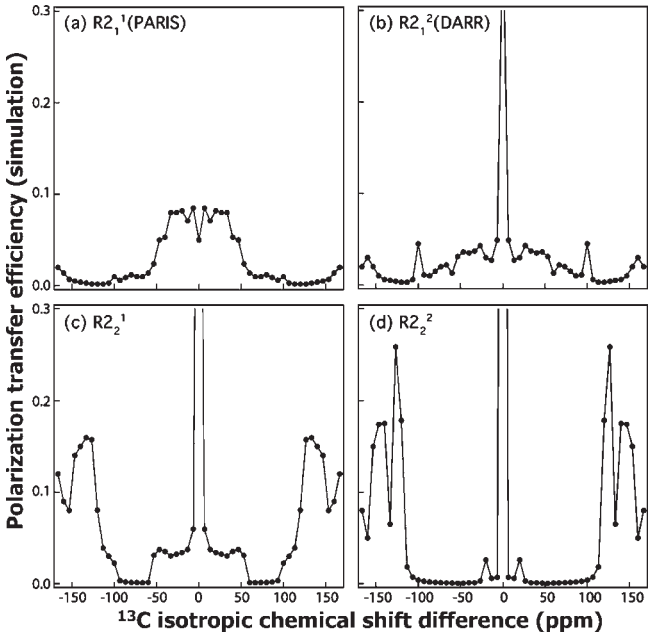

Figure 8. Simulated dependence of the $^{13}C-^{13}C$ polarization transfer efficiency on the isotropic chemical shift difference for various $R2_n^\nu$ symmetry sequences: (a) $R2_1^1$, (b) $R2_1^2$ (DARR), (c) $R2_2^1$, and (d) $R2_2^2$. The simulations were performed in SIMPSON, and the model spin systems contained 2 protons and 2 carbons. The MAS frequency was 40 kHz, and the mixing time was 4 ms. Note that the simulated resonance frequency offsets are ±25 kHz covering the entire spectral range for ^{13}C at a magnetic field of 14.1 T.

strength, the chemical shift difference, and the size of the recoupled dipolar interactions as well. On the other hand, even though the other $R2_n^\nu$ sequences also depend significantly on the chemical shift differences of coupled carbons, each of these experiments exhibits high recoupling efficiency for either $C_\alpha-C_\beta$ or $C_\alpha-C'$ correlations, suggesting that with a pair of experiments, $R2_1^1$ and $R2_2^2$, both types of correlations can be recorded. Alternatively, if a single experiment is desirable to achieve both $C_\alpha-C_\beta$ and $C_\alpha-C'$ correlations, the $R2_2^1$ symmetry sequence can be used. Although this experiment does not exhibit the highest transfer efficiencies for either $C_\alpha-C_\beta$ or $C_\alpha-C'$ correlations, the transfer efficiency is still high enough to attain high sensitivity and uniform excitation for both spectral regions.

To further evaluate the experimental results, we examined the dependence of chemical shift difference on the polarization transfer dynamics at fast and moderate MAS frequencies by numerical simulations. Figure 8 illustrates the simulated dependence of the $^{13}C-^{13}C$ polarization transfer efficiency on the chemical shift difference for $R2_1^2$, $R2_1^1$, $R2_2^2$, and $R2_2^1$ sequences at the MAS frequency of 40 kHz. It can be noted that the $R2_1^1$ symmetry scheme exhibits relatively high polarization transfer efficiency for the coupled ^{13}C spins with small chemical shift differences (of less than 47 ppm). This indicates that the $R2_1^1$ symmetry sequence is suitable for recording $C_\alpha-C_\beta$, $C_\beta-C_\gamma$, and other side chain correlations in spin diffusion experiments. On the other hand, essentially no polarization transfer is expected for the coupled ^{13}C spins with chemical shift differences larger than 50 ppm in the $R2_1^1$ experiment, while DARR (the $R2_1^2$ sequence) results in very weak polarization transfer. At the same time, the $R2_2^2$ and $R2_2^1$ symmetry sequences give rise to much higher transfer efficiencies for correlations between coupled carbons with large chemical shift differences, such as $C_\alpha-C'$ spin pairs whose chemical shift differences are of the order of 120 ppm, even multibond $C_{\beta/\gamma}-C'$ spin pairs with chemical shift differences of 120−170 ppm. This simulated behavior agrees well with the experimental results presented in Figures 5 and 7.

It is obvious from the above that the polarization transfer under very fast MAS can be driven by the $R2_n^\nu$ recoupled dipolar interactions when the second-order rotational resonance conditions are fulfilled, $\omega_1 \pm n\omega_r - K_{sc}\omega_{DD} \leq \Delta\omega_{iso} \leq \omega_1 \pm n\omega_r + K_{sc}\omega_{DD}$, where $K_{sc}\omega_{DD}$ denotes the scaled dipolar couplings reintroduced by $R2_n^\nu$ symmetry sequences. However, even when these conditions are fulfilled, it is still difficult to obtain a true broad-band recoupling. The transfer efficiency is dependent on the chemical shift difference, and it is therefore anticipated that the polarization transfer profile will be dependent on the magnetic field strength. Even though we have not yet performed R-type spin diffusion experiments at magnetic field strengths other than 14.1 T, the magnetic field dependence of the performance of these sequences can be understood by the analysis of Figure 8. The simulated dependence of the chemical shift difference reveals the conditions where strong vs no correlations would be observed for each $R2_n^\nu$ sequence. For instance, at the MAS frequency of 40 kHz, for the $R2_2^1$ sequence there will be no correlations for coupled ^{13}C nuclei with chemical shift differences of 9−14 kHz. Translating the CS difference into ppm, we realize that no correlations are expected between the coupled ^{13}C spins with the chemical shift differences of 90−140 ppm at 9.4 T, of 60−90 ppm at 14.1 T (as confirmed experimentally in this work), and of 40−60 ppm at 21.1 T. In other words and considering that the R2-driven spin diffusion is accomplished by the second-order rotational resonance conditions, the above considerations imply that the correlation information for the desired chemical shift differences, i.e., aliphatic-to-carbonyl or aliphatic-to-aliphatic regions in proteins, can be obtained at each magnetic field by an appropriate setting of the MAS frequency for each $R2_n^\nu$ sequence, i.e., 30 kHz at 9.4 T, 40 kHz at 14.1 T, and 60 kHz at 21.1 T.

Indeed, numerical simulations of the dependence of the polarization transfer efficiencies on the chemical shift differences for each $R2_n^\nu$ sequence conducted for the magnetic field strength of 21.1 T and the MAS frequency of 60 kHz demonstrate that the transfer profiles (see Figure S4 of the Supporting Information) are in agreement with the above analysis, which was made on the basis of the simulations at 14.1 T and 40 kHz.

At moderate MAS frequencies (<20 kHz), the numerical simulations indicate that the polarization transfer dynamics is only mildly dependent on the chemical shift differences, except for the rotational resonance conditions (see Supporting Information). Therefore, broad-band homonuclear recoupling can be easily achieved by each of the four $R2_n^\nu$ schemes, confirming our experimental observations. This behavior is expected to hold at moderate MAS frequencies for any magnetic field strength practically accessible in a modern NMR spectrometer.

Symmetry-Based Spin Diffusion Experiments at Very Fast MAS Frequencies: Applications to Proteins and Protein Assemblies. As discussed in the previous sections, at very fast MAS frequencies where DARR ($R2_1^2$) experiment fails, the other $R2_n^\nu$ symmetry sequences are expected to result in efficient polarization transfer and therefore should be useful for $^{13}C-^{13}C$ homonuclear correlation spectroscopy of proteins.

dx.doi.org/10.1021/ja108650x |J. Am. Chem. Soc. 2011, 133, 3943–3953

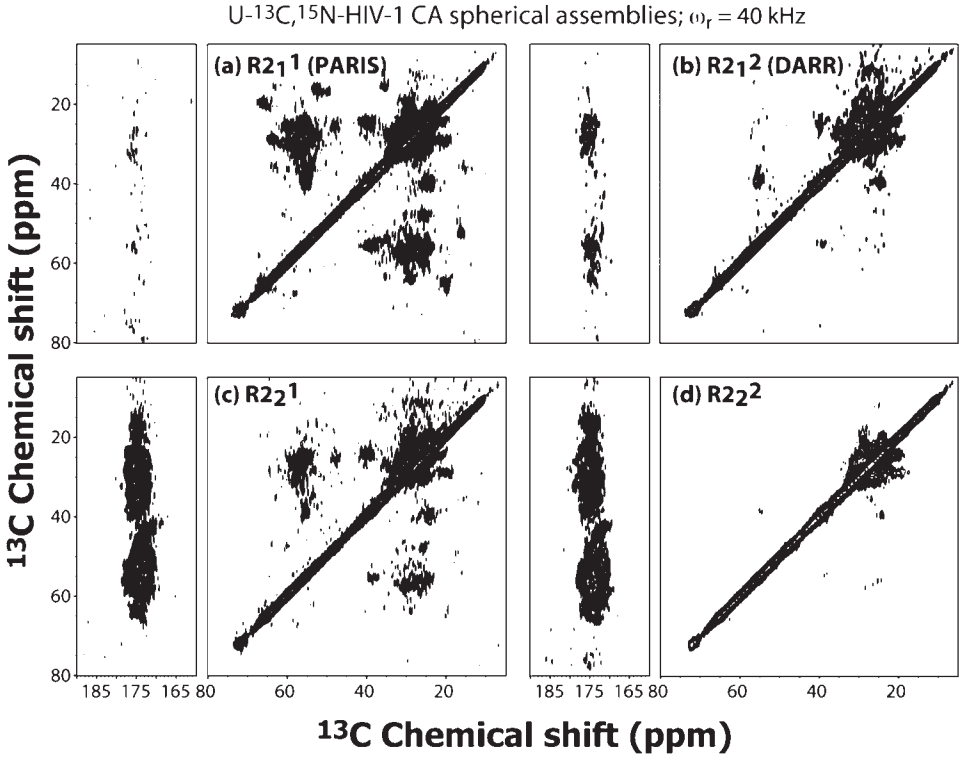

Figure 9. 2D $^{13}C-^{13}C$ correlation spectra of spherical assemblies of U$-^{13}C,^{15}N$-enriched HIV-1 CA, recorded at 14.1 T with the different $R2_n^{\nu}$ sequences: (a) $R2_1^1$, (b) $R2_1^2$, (c) $R2_2^1$, and (d) $R2_2^2$. A mixing time of 250 ms was used to record each spectrum. The sample was spun at a MAS frequency of 40 kHz. CW ^1H decoupling (ω_1 = 9 kHz) was employed in the t_1 and t_2 dimensions.

In Figure 9 we provide the 14.1 T $^{13}C-^{13}C$ correlation spectra using the various $R2_n^{\nu}$ symmetry schemes for spherical assemblies of U$-^{13}C,^{15}N$-enriched HIV-1 CA capsid protein, spun at the MAS frequency of 40 kHz. We note that it is of great interest to further characterize the structure and dynamic properties of this morphology since it relates to the assembly in the immature HIV-1 virions. At the same time, the inherently limited spectral resolution of the spherical assemblies at moderate MAS frequencies (see Supporting Information showing a 10 kHz DARR spectrum) so far made their solid-state NMR studies challenging.

As illustrated in Figure 9 b, at 40 kHz the DARR spectrum exhibits only a few cross peaks, even at a mixing time as long as 250 ms. Notably, even cross peaks for directly bonded carbons are not observed in the spectrum, confirming that DARR fails under very fast MAS conditions in proteins. On the other hand, the $R2_1^1$ correlation spectrum displayed in Figure 9 a contains a large number of cross peaks in the aliphatic region. However, almost no aliphatic-to-carbonyl correlations are seen, illustrating the inefficient recoupling of the carbon spin pairs with large chemical shift differences by this sequence. Conversely, Figure 9 d illustrates that the $R2_2^2$ symmetry irradiation results in very efficient recoupling between the carbonyl and the aliphatic carbons with large chemical shift differences, while the polarization transfer within the aliphatic carbons is very weak. The most uniform polarization transfer is achieved by the $R2_2^1$ irradiation, and the corresponding spectrum is provided in Figure 9 c, exhibiting cross peaks over the entire spectral range. At the same time, the polarization transfer efficiency for spin diffusion within the aliphatic carbons is about 70% of that in the $R2_1^1$ symmetry-driven experiment. This is consistent with the numerical simulations presented in Figure 8 and with the model experiments on alanine presented in Figure 7, which show the second highest polarization transfer efficiency for the $R2_2^1$ symmetry scheme among all $R2_n^{\nu}$ sequences, for both aliphatic-to-aliphatic and carbonyl-to-aliphatic carbons. Therefore, the combined results provided in Figure 9 demonstrate that the $R2_2^2$, $R2_2^1$, and $R2_1^1$ symmetry-driven spin diffusion experiments are efficient for $^{13}C-^{13}C$ correlation spectroscopy in proteins and can be used in place of DARR at very fast MAS frequencies.

Another observation made on the basis of the experimental $^{13}C-^{13}C$ spin diffusion spectra of spherical HIV-1 CA assemblies acquired at 40 and 10 kHz is that the 40 kHz R2-based spectra exhibit higher resolution (as illustrated in Figure S6 of the Supporting Information). To further test this experimental observation, we carried out R2-based experiments for U$-^{13}$C,^{15}N-enriched DLC8 protein. The resulting 2D $^{13}C-^{13}C$ correlation spectra acquired with MAS frequencies of 10 (DARR) and 40 kHz ($R2_1^1$) are shown in Figure 10. As can be appreciated, the $R2_1^1$ correlation spectrum recorded at ω_r = 40 kHz (Figure 10 b) exhibits significantly higher resolution without any loss of the correlation information, compared to the DARR spectrum at 10 kHz. The 1D slices extracted along the ω_1 and ω_2 frequency dimensions of the 2D spectra (Figure 10 c and 10d) clearly demonstrate that the lines are narrower along both frequency dimensions at the MAS frequency of 40 kHz, even when low-power CW ^1H decoupling with the rf field strength of 9 kHz was performed. This resolution gain is also obvious in the comparison of the frequency domains of the indirect (ω_1) dimensions of the 40 and 10 kHz R2 and DARR spectra (see Supporting Information).

$R2_n^{\nu}$-driven spin diffusion experiments were also conducted on the sparsely-^{13}C, U$-^{15}N$-enriched CAP-Gly domain of

dx.doi.org/10.1021/ja108650x |J. Am. Chem. Soc. 2011, 133, 3943–3953

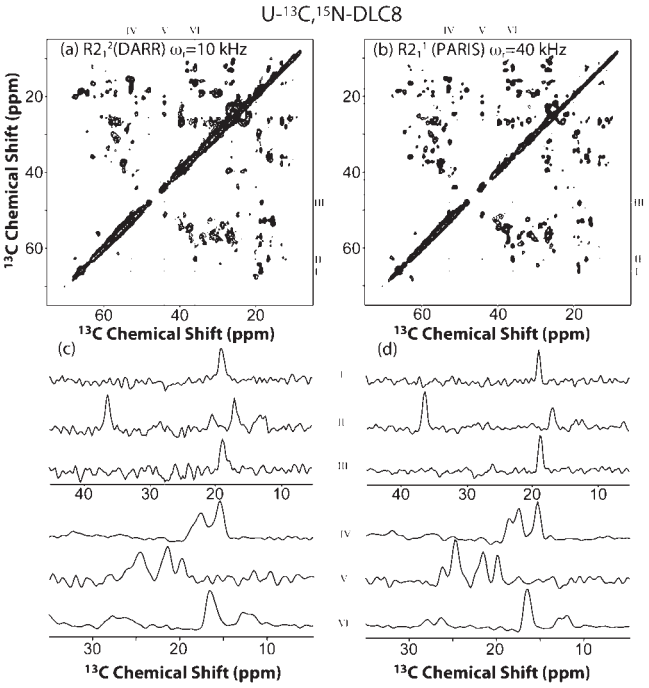

Figure 10. Comparison of the aliphatic region of the 2D $^{13}C-^{13}C$ correlation spectra recorded on U$-^{13}C,^{15}N$-enriched DLC8. (a) $R2_1^2$ (DARR) spectrum of the sample spun at 10 kHz; high-power TPPM ^1H decoupling with $\omega_1 = 96$ kHz was employed in the t_1 and t_2 dimensions. (b) $R2_1^1$ spectrum of the sample spun at 40 kHz; low-power CW ^1H decoupling ($\omega_1 = 9$ kHz) was employed in the t_1 and t_2 dimensions. Mixing times of 20 and 200 ms were used to record the DARR spectrum at 10 kHz and the $R2_1^1$ spectrum at 40 kHz, respectively. (c and d) 1D slices extracted along the ω_2 (I−III) and ω_1 (IV−VI) frequency dimensions of the 2D $^{13}C-^{13}C$ correlation spectra. The first contour in all spectra is set at $5 \times \sigma$ (σ is the noise rmsd) with a multiplier of 1.2.

dynactin in which only few neighboring ^{13}C atoms are enriched (for enrichment pattern, see refs 72−74). Figure 11 displays the 2D $^{13}C-^{13}C$ correlation spectra with the various $R2_n^\nu$ symmetry schemes at the MAS frequency of 40 kHz. As can be appreciated, excellent resolution is seen and the correlation information as well as the transfer efficiencies using the various $R2_n^\nu$ sequences for the sparsely labeled CAP-Gly sample are consistent with those obtained for HIV-1 CA protein assemblies and DLC8. Interestingly, in the case of the sparsely enriched CAP-Gly protein, no appreciable resolution enhancements were noted for the MAS frequency of 40 kHz compared to the 10 kHz spectra (see Supporting Information), suggesting that considerable contributions to the linewidths in the 10 kHz spectra of the uniformly enriched proteins are due to $^{13}C-^{13}C$ dipolar and $^{13}C-^{15}N$ scalar couplings.

Overall, the above results on model compounds and on three different protein samples demonstrate that $R2_2^2$, $R2_2^1$, and $R2_1^1$ experiments perform well at very fast MAS rates, while DARR and PDSD sequences fail. These $R2_2^2$, $R2_2^1$, and $R2_1^1$ experiments not only have high transfer efficiencies but also display greatly enhanced spectral resolution for uniformly enriched samples under very fast MAS conditions. Both of these features are critically important in multidimensional experiments for resonance assignments and measurements of distance restraints in large proteins and protein assemblies in both uniformly labeled and sparsely or selectively labeled samples.

CONCLUSIONS

In summary, we describe a family of rotor-synchronized $R2_n^\nu$ symmetry sequences for homonuclear correlation spectroscopy in rotating solids in which $R2_1^1$, $R2_1^2$, $R2_2^1$, or $R2_2^2$ irradiation is applied to the proton spins during the mixing time to assist $^{13}C-^{13}C$ polarization transfer. Three of these R2-driven spin diffusion sequences (RDSD), $R2_1^1$, $R2_2^1$, and $R2_2^2$, work efficiently at both moderate and fast MAS frequencies. Our results indicate that RDSD sequences exhibit similar transfer efficiencies at moderate MAS rates (up to 20 kHz) and that $R2_1^1$ and POST $R2_2^1$ sequences are superior for the recoupling of coupled spins that possess large chemical shift differences, such as carbonyl-to-aliphatic carbons. At very fast MAS frequencies (40 kHz), where the PDSD and DARR ($R2_1^2$) experiments fail, the $R2_2^2$, $R2_2^1$, and $R2_1^1$ sequences exhibit high polarization transfer efficiencies. Since the broadened second-order rotational resonance conditions ($\omega_1 \pm n\omega_r - K_{sc}\omega_{DD} \leq \Delta\omega_{iso} \leq \omega_1 \pm n\omega_r + K_{sc}\omega_{DD}$) are dominated by the rf field strength and the size of the reintroduced dipolar interactions, these symmetry-based experiments exhibit different dependencies on the chemical shift differences between coupled spins. The $R2_1^1$ sequence is most efficient for recoupling of the carbons with small chemical shift differences, while the $R2_2^2$ sequence shows highest polarization transfer efficiencies for coupled spins with large chemical shift differences. The $R2_2^1$ symmetry sequence displays high transfer efficiency and uniform excitation for both aliphatic-to-aliphatic and carbonyl-to-aliphatic correlations (see the summary figure in the Supporting Information). With the replacement of the basic π pulse by various composite pulses, the appropriate POST $R2_n^\nu$ symmetry sequences are expected to give faster transfer rate and higher transfer efficiency. Given the advantageous properties of the $R2_n^\nu$ symmetry-based spin diffusion schemes introduced here, we believe that they will become indispensible for resonance assignments and structure determination of proteins and protein assemblies.

ASSOCIATED CONTENT

Supporting Information. Tables with (1) details of the recoupled first-order average Hamiltonian terms by $R2_n^\nu$ symmetry sequences and (2) detailed acquisition and processing parameters for 2D $^{13}C-^{13}C$ RDSD experiments on HIV-1 CA protein, DLC8, and CAP-Gly samples; Figures displaying (1) 1D ^{13}C CP/MAS experiments of [U$-^{13}C,^{15}N$]-MLF spun at 10 kHz with $R2_n^\nu$ symmetry irradiation, (2) 1D polarization transfer experiments from C_α and C_β to C′ carbons of MLF with different $R2_n^\nu$ irradiation, spun at 10 kHz, (3) 1D polarization transfer experiments from C_α and C_β to the C′ carbon of alanine with different $R2_n^\nu$ irradiation, spun at 40 kHz, (4) SIMPSON simulations on the chemical shift offset dependence of the polarization transfer efficiency at a MAS rate of 60 kHz and magnetic field of 21.1 T, (5) SIMPSON simulations on the chemical shift offset dependence of the polarization transfer efficiency at a MAS rate of 10 kHz, (6) Comparison of the 2D $^{13}C-^{13}C$ correlation spectra of spherical assemblies of U$-^{13}C,^{15}N$-enriched HIV-1 CA protein acquired at 10 kHz and 40 kHz, (7) Stack plots of the aliphatic regions of the 2D $^{13}C-^{13}C$ correlation spectra recorded on U$-^{13}C,^{15}N$-enriched DLC8, (8) Comparison of the aliphatic region of the 2D $^{13}C-^{13}C$ correlation spectra recorded for sparsely-^{13}C, U$-^{15}N$-enriched CAP-Gly at MAS frequencies of 10 and 40 kHz, (9) Comparison of

dx.doi.org/10.1021/ja108650x |J. Am. Chem. Soc. 2011, 133, 3943–3953

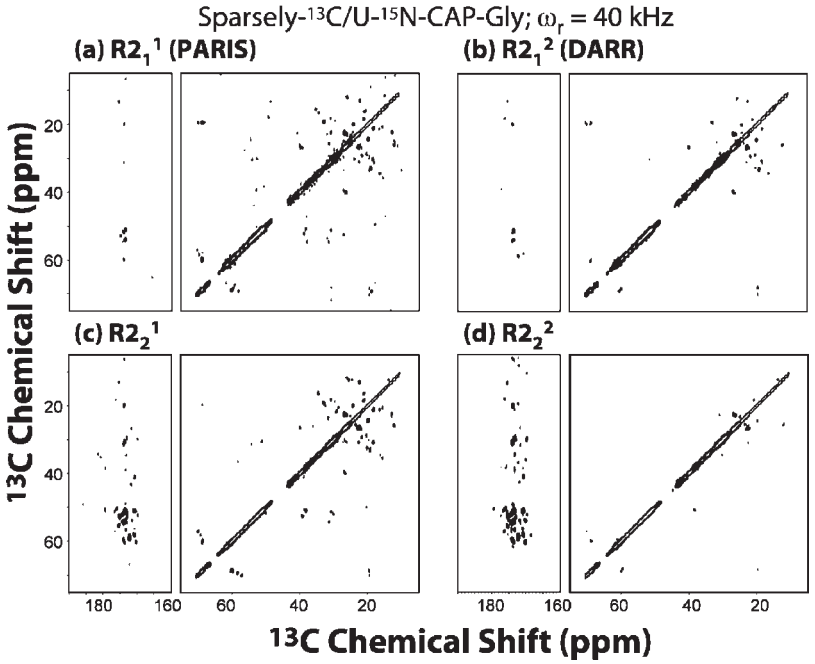

Figure 11. 2D $^{13}C-^{13}C$ correlation spectra of sparsely-^{13}C, U$-^{15}N$-enriched CAP-Gly domain of dynactin. The spectra were acquired at 14.1 T with the different $R2_n^{\nu}$ sequences: (a) $R2_1^1$, (b) $R2_1^2$, (c) $R2_2^1$, and (d) $R2_2^2$. Each spectrum was recorded with a mixing time of 300 ms, and the sample was spun at a MAS frequency of 40 kHz. The 2D spectra were collected as (1000 × 200) (complex × real) matrices with 128 scans; TPPI scheme was used for phase-sensitive detection in the indirect dimension. Low-power CW ^1H decoupling ($\omega_1 = 9$ kHz) was employed in the t_1 and t_2 dimensions. The first contour in all spectra is set at 5 × σ (σ is the noise rmsd) with a multiplier of 1.2.

^{13}C polarization delays along the t_1 time domain, extracted from R2 experiments at 10 and 40 kHz on U$-^{13}C,^{15}N$-enriched DLC8, (10) Summary of optimal applicability regimes for the various $R2_n^{\nu}$ sequences at a MAS frequency of 40 kHz. This material is available free of charge via the Internet at http://pubs.acs.org.

AUTHOR INFORMATION

Corresponding Author
tpolenov@udel.edu

ACKNOWLEDGMENT

This work was supported by the National Institutes of Health (NIGMS Grants P50GM082251-03 and R01GM085396; NCRR grants P20RR015588-10 and 5P20RR017716-07) and is a contribution from the Pittsburgh Center for HIV Protein Interactions.

REFERENCES

(1) Tycko, R. *Prog. Nucl. Magn. Reson. Spectrosc.* **2003**, *42*, 53–68.
(2) Petkova, A. T.; Ishii, Y.; Balbach, J. J.; Antzutkin, O. N.; Leapman, R. D.; Delaglio, F.; Tycko, R. *Proc. Natl. Acad. Sci. U.S.A.* **2002**, *99*, 16742–16747.
(3) Ma, C.; Marassi, F. M.; Jones, D. H.; Straus, S. K.; Bour, S.; Strebel, K.; Schubert, U.; Oblatt-Montal, M.; Montal, M.; Opella, S. J. *Protein Sci.* **2002**, *11*, 546–557.
(4) Nishimura, K.; Kim, S.; Zhang, L.; Cross, T. A. *Biochemistry* **2002**, *41*, 13170–13177.
(5) Lorieau, J. L.; Day, L. A.; McDermott, A. E. *Proc. Natl. Acad. Sci. U.S.A.* **2008**, *105*, 10366–10371.
(6) Han, Y.; Ahn, J.; Concel, J.; Byeon, I. J.; Gronenborn, A. M.; Yang, J.; Polenova, T. *J. Am. Chem. Soc.* **2010**, *132*, 1976–1987.
(7) Sun, S.; Siglin, A.; Williams, J. C.; Polenova, T. *J. Am. Chem. Soc.* **2009**, *131*, 10113–10126.
(8) Xu, J.; Durr, U. H.; Im, S. C.; Gan, Z.; Waskell, L.; Ramamoorthy, A. *Angew. Chem., Int. Ed. Engl.* **2008**, *47*, 7864–7867.
(9) Qiang, W.; Bodner, M. L.; Weliky, D. P. *J. Am. Chem. Soc.* **2008**, *130*, 5459–5471.
(10) Franks, W. T.; Wylie, B. J.; Stellfox, S. A.; Rienstra, C. M. *J. Am. Chem. Soc.* **2006**, *128*, 3154–3155.
(11) Sun, B. Q.; Rienstra, C. M.; Costa, P. R.; Williamson, J. R.; Griffin, R. G. *J. Am. Chem. Soc.* **1997**, *119*, 8540–8546.
(12) Rienstra, C. M.; Hohwy, M.; Hong, M.; Griffin, R. G. *J. Am. Chem. Soc.* **2000**, *122*, 10979–10990.
(13) Baldus, M. *Prog. Nucl. Magn. Reson. Spectrosc.* **2002**, *41*, 1–47.
(14) Jaroniec, C. P.; Filip, C.; Griffin, R. G. *J. Am. Chem. Soc.* **2002**, *124*, 10728–10742.
(15) Igumenova, T. I.; McDermott, A. E. *J. Magn. Reson.* **2005**, *175*, 11–20.
(16) Tian, Y.; Chen, L.; Niks, D.; Kaiser, J. M.; Lai, J.; Rienstra, C.; Dunn, M. F.; Mueller, L. *Phys. Chem. Chem. Phys.* **2009**, *11*, 7078–7086.
(17) Chen, L.; Kaiser, J. M.; Polenova, T.; Yang, J.; Rienstra, C.; Mueller, L. *J. Am. Chem. Soc.* **2007**, *129*, 10650–10651.
(18) Bennett, A. E.; Ok, J. H.; Griffin, R. G.; Vega, S. *J. Chem. Phys.* **1992**, *96*, 8624–8627.
(19) Verel, R.; Ernst, M.; Meier, B. H. *J. Magn. Reson.* **2001**, *150*, 81–99.
(20) Takegoshi, K.; Nakamura, S.; Terao, T. *Chem. Phys. Lett.* **2001**, *344*, 631–637.
(21) Baldus, M.; Petkova, A. T.; Herzfeld, J.; Griffin, R. G. *Mol. Phys.* **1998**, *95*, 1197–1207.
(22) McDermott, A.; Polenova, T.; Bockmann, A.; Zilm, K. W.; Paulson, E. K.; Martin, R. W.; Montelione, G. T. *J. Biomol. NMR* **2000**, *16*, 209–219.
(23) Pauli, J.; Baldus, M.; van Rossum, B.; de Groot, H.; Oschkinat, H. *ChemBioChem* **2001**, *2*, 272–281.
(24) Hou, G.; Paramasivam, S.; Byeon, I. J.; Gronenborn, A. M.; Polenova, T. *Phys. Chem. Chem. Phys.* **2010**, *12*, 14873–14883.

(25) Samoson, A.; Tuherm, T.; Gan, Z. *Solid State Nucl. Magn. Reson.* **2001**, *20*, 130–136.
(26) Ernst, M.; Meier, M. A.; Tuherm, T.; Samoson, A.; Meier, B. H. *J. Am. Chem. Soc.* **2004**, *126*, 4764–4765.
(27) Samoson, A.; Tuherm, T.; Past, J.; Reinhold, A.; Anupold, T.; Heinmaa, N. *New Tech. Solid-State NMR* **2005**, *246*, 15–31.
(28) Reif, B.; Jaroniec, C. P.; Rienstra, C. M.; Hohwy, M.; Griffin, R. G. *J. Magn. Reson.* **2001**, *151*, 320–327.
(29) Zhou, D.; Shea, J.; Nieuwkoop, A.; Franks, W.; Wylie, B.; Mullen, C.; Sandoz, D.; Rienstra, C. *Angew. Chem., Int. Ed.* **2007**, *46*, 8380–8383.
(30) Zhou, D. H.; Shah, G.; Cormos, M.; Mullen, C.; Sandoz, D.; Rienstra, C. *J. Am. Chem. Soc.* **2007**, *129*, 11791–11801.
(31) Zhou, D.; Shah, G.; Mullen, C.; Sandoz, D.; Rienstra, C. *Angew. Chem., Int. Ed.* **2009**, *48*, 1253–1256.
(32) Ernst, M.; Detken, A.; Bockmann, A.; Meier, B. H. *J. Am. Chem. Soc.* **2003**, *125*, 15807–15810.
(33) Herbst, C.; Herbst, J.; Kirschstein, A.; Leppert, J.; Ohlenschläger, O.; Görlach, M.; Ramachandran, R. *J. Biomol. NMR* **2009**, *43*, 51–61.
(34) Lewandowski, J. R.; De Paepe, G.; Eddy, M.; Griffin, R. *J. Am. Chem. Soc.* **2009**, *131*, 5769–5776.
(35) Lewandowski, J. R.; De Paepe, G.; Griffin, R. *J. Am. Chem. Soc.* **2007**, *129*, 728–729.
(36) Scholz, I.; Huber, M.; Manolikas, T.; Meier, B.; Ernst, M. *Chem. Phys. Lett.* **2008**, *460*, 278–283.
(37) Bloembergen, N. *Physica* **1949**, *15*, 386–426.
(38) Meier, B. H., . *Advances in Magnetic and Optical Resonance*; Academic Press: New York, 1994.
(39) Takegoshi, K.; Nakamura, S.; Terao, T. *J. Chem. Phys.* **2003**, *118*, 325–2341.
(40) Morcombe, C. R.; Gaponenko, V.; Byrd, R. A.; Zilm, K. W. *J. Am. Chem. Soc.* **2004**, *126*, 7196–7197.
(41) Hong, M. *J. Phys. Chem. B* **2007**, *111*, 10340–10351.
(42) Loquet, A.; Bardiaux, B.; Gardiennet, C.; Blanchet, C.; Baldus, M.; Nilges, M.; Malliavin, T.; Böckmann, A. *J. Am. Chem. Soc.* **2008**, *130*, 3579–3589.
(43) McDermott, A.; Polenova, T. *Curr. Opin. Struct. Biol.* **2007**, *17*, 617–622.
(44) Yang, J.; Paramasivam, S.; Marulanda, D.; Cataldi, M.; Tasayco, M. L.; Polenova, T. *Magn. Reson. Chem.* **2007**, *45*, 73–83.
(45) Yang, J.; Tasayco, M. L.; Polenova, T. *J. Am. Chem. Soc.* **2008**, *130*, 5798–5807.
(46) Marulanda, D.; Tasayco, M. L.; McDermott, A.; Cataldi, M.; Arriaran, V.; Polenova, T. *J. Am. Chem. Soc.* **2004**, *126*, 16608–16620.
(47) Jehle, S.; Hiller, M.; Rehbein, K.; Diehl, A.; Oschkinat, H.; Rossum, B. *J. Biomol. NMR* **2006**, *36*, 169–177.
(48) Higman, V.; Flinders, J.; Hiller, M.; Jehle, S.; Markovic, S.; Fiedler, S.; Rossum, B.; Oschkinat, H. *J. Biomol. NMR* **2009**, *44*, 245–260.
(49) Franks, W. T.; Zhou, D. H.; Wylie, B. J.; Money, B. G.; Graesser, D. T.; Frericks, H. L.; Sahota, G.; Rienstra, C. M. *J. Am. Chem. Soc.* **2005**, *127*, 12291–12305.
(50) Rienstra, C. M.; Tucker-Kellogg, L.; Jaroniec, C. P.; Hohwy, M.; Reif, B.; McMahon, M. T.; Tidor, B.; Lozano-Perez, T.; Griffin, R. G. *Proc. Natl. Acad. Sci. U.S.A.* **2002**, *99*, 10260–10265.
(51) Siemer, A.; Ritter, C.; Ernst, M.; Riek, R.; Meier, B. *Angew. Chem., Int. Ed.* **2005**, *44*, 2441–2444.
(52) Nadaud, P.; Helmus, J.; Hofer, N.; Jaroniec, C. *J. Am. Chem. Soc.* **2007**, *129*, 7502–7503.
(53) Nadaud, P.; Helmus, J.; Kall, S. L.; Jaroniec, C. *J. Am. Chem. Soc.* **2009**, *131*, 8108–8120.
(54) Weingarth, M.; Bodenhausen, G.; Tekely, P. J. *Am. Chem. Soc.* **2009**, *131*, 13937–13938.
(55) Xu, J.; Struppe, J.; Ramamoorthy, A. J. *Chem. Phys.* **2008**, *128*, 052308.
(56) Hou, G.; Deng, F.; Ye, C.; Ding, S. *J. Chem. Phys.* **2006**, *124*, 234512.
(57) Hou, G.; Ding, S.; Zhang, L.; Deng, F. *J. Am. Chem. Soc.* **2010**, *132*, 5538–5539.
(58) De Paëpe, G.; Lewandowski, J.; Loquet, A.; Böckmann, A.; Griffin, R. *J. Chem. Phys.* **2008**, *129*, 245101.
(59) Lewandowski, J. R.; De Paepe, G.; Eddy, M.; Struppe, J.; Maas, W.; Griffin, R. *J. Phys. Chem. B* **2009**, *113*, 9062–9069.
(60) Lange, A.; Luca, S.; Baldus, M. *J. Am. Chem. Soc.* **2002**, *124*, 9704–9705.
(61) Lange, A.; Seidel, K.; Verdier, L.; Luca, S.; Baldus, M. *J. Am. Chem. Soc.* **2003**, *125*, 12640–12648.
(62) Marulanda, D.; Tasayco, M. L.; Cataldi, M.; Arriaran, V.; Polenova, T. *J. Phys. Chem. B* **2005**, *109*, 18135–18145.
(63) Grommek, A.; Meier, B. H.; Ernst, M. *Chem. Phys. Lett.* **2006**, *427*, 404–409.
(64) Bayro, M. J.; Huber, M.; Ramachandran, R.; Davenport, T. C.; Meier, B. H.; Ernst, M.; Griffin, R. G. J. *Chem. Phys.* **2009**, *130*, 114506.
(65) Duma, L.; Abergel, D.; Ferrage, F.; Pelupessy, P.; Tekely, P.; Bodenhausen, G. *Chem. Phys. Chem.* **2008**, *9*, 1104–1106.
(66) Weingarth, M.; Demco, D. E.; Bodenhausen, G.; Tekely, P. *Chem. Phys. Lett.* **2009**, *469*, 342–348.
(67) Weingarth, M.; Bodenhausen, G.; Tekely, P. *Chem. Phys. Lett.* **2010**, *488*, 10–16.
(68) Levitt, M. H. . *Encyclopedia of Nuclear Magnetic Resonance: Supplementary Vol.*; Grant, D. M., Harris, R. K., Eds.; Wiley: Chichester, U.K., 2002.
(69) Carravetta, M.; Eden, M.; Zhao, X.; Brinkmann, A.; Levitt, M. H. *Chem. Phys. Lett.* **2000**, *321*, 205–215.
(70) Brinkmann, A.; Levitt, M. H. *J. Chem. Phys.* **2001**, *115*, 357–384.
(71) Brinkmann, A.; Kentgens, A. P.; Anupold, T.; Samoson, A. *J. Chem. Phys.* **2008**, *129*, 174507.
(72) LeMaster, D. M.; Kushlan, D. M. *J. Am. Chem. Soc.* **1996**, *118*, 9255–9264.
(73) Castellani, F.; van Rossum, B.; Diehl, A.; Schubert, M.; Rehbein, K.; Oschkinat, H. *Nature* **2002**, *420*, 98–102.
(74) Hiller, M.; Higman, V. A.; Jehle, S.; van Rossum, B. J.; Kuhlbrandt, W.; Oschkinat, H. *J. Am. Chem. Soc.* **2008**, *130*, 408–409.
(75) Lightcap, C. M.; Sun, S.; Lear, J. D.; Rodeck, U.; Polenova, T.; Williams, J. C. *J. Biol. Chem.* **2008**, *283*, 27314–27324.
(76) Bennett, A. E.; Rienstra, C. M.; Auger, M.; Lakshmi, K. V.; Griffin, R. G. *J. Chem. Phys.* **1995**, *103*, 6951–6958.
(77) Marion, D.; Wuthrich, K. *Biochem. Biophys. Res. Commun.* **1983**, *113*, 967–974.
(78) Bak, M.; Rasmussen, J. T.; Nielsen, N. C. *J. Magn. Reson.* **2000**, *147*, 296–330.